catalysts

MDPI

Article

Highly Efficient Visible Light Photodegradation of Cr(VI) Using Electrospun MWCNTs-Fe_3O_4@PES Nanofibers

Alaa Mohamed [1,*], Samy Yousef [2,3], Shady Ali [1], Mantas Sriubas [4], Sarunas Varnagiris [5], Simona Tuckute [5], Mohammed Ali Abdelnaby [6] and Bahaa M. Kamel [7]

1 Department of Mechatronics, Canadian International College, Fifth Settlement, New Cairo 11865, Egypt; shady_rabei@cic-cairo.com
2 Department of Production Engineering, Faculty of Mechanical Engineering and Design, Kaunas University of Technology, LT-51424 Kaunas, Lithuania; ahmed.saed@ktu.lt
3 Department of Materials Science, South Ural State University, Lenin Prospect 76, 454080 Chelyabinsk, Russia
4 Physics Department, Kaunas University of Technology, LT-51368 Kaunas, Lithuania; mantas.sriubas@ktu.lt
5 Center for Hydrogen Energy Technologies, Lithuanian Energy Institute, Breslaujos 3, 44403 Kaunas, Lithuania; sarunas.varnagiris@ktu.lt (S.V.); simona.tuckute@ktu.lt (S.T.)
6 Production Engineering and Printing Technology Department, Akhbar El Yom Academy, Giza 12655, Egypt; Muhmmad.aly@akhbaracademy.edu.eg
7 Mechanical Engineering Department, National Research Centre, Giza 12622, Egypt; bahaa2004eg@yahoo.com
* Correspondence: alakha@kth.se

Abstract: The development of highly efficient photocatalysis has been prepared by two different methods for the photodegradation of Cr(VI) from an aqueous solution under visible light. The electrospun polyethersulfone (PES)/iron oxide (Fe_3O_4) and multi-wall carbon nanotubes (MWCNTs) composite nanofibers have been prepared using the electrospinning technique. The prepared materials were characterized by SEM and XRD analysis. The result reveals the successful fabrication of the composite nanofiber with uniformly and smooth nanofibers. The effect of numerous parameters were explored to investigate the effects of pH value, contact time, concentration of Cr(VI), and reusability. The MWCNTs-Fe_3O_4@PES composite nanofibers exhibited excellent photodegradation of Cr(VI) at pH 2 in 80 min. The photocatalysis materials are highly stable without significant reduction of the photocatalytic efficiency of Cr(VI) after five cycles. Therefore, due to its easy separation and reuse without loss of photocatalytic efficiency, the photocatalysis membrane has tremendous potential for the removal of heavy metals from aqueous solutions.

Keywords: iron oxide; MWCNTs; photocatalysis; Cr(VI); visible light

Citation: Mohamed, A.; Yousef, S.; Ali, S.; Sriubas, M.; Varnagiris, S.; Tuckute, S.; Abdelnaby, M.A.; Kamel, B.M. Highly Efficient Visible Light Photodegradation of Cr(VI) Using Electrospun MWCNTs-Fe_3O_4@PES Nanofibers. *Catalysts* **2021**, *11*, 868. https://doi.org/10.3390/catal11070868

Academic Editors: Ioannis Konstantinou and Ekaterina A. Kozlova

Received: 9 June 2021
Accepted: 19 July 2021
Published: 20 July 2021

1. Introduction

Heavy metal pollution is one of the most serious environmental and public health issues. Chromium is one of the most dangerous heavy metals, and it has been used in a variety of industries, such as dyes, textiles, leather tanning, electroplating, and alloying [1,2]. Cr(VI) and Cr(III) are the two oxidation states of chromium, where Cr(VI) is more toxic to humans than Cr(III) with high stability, toxicity, and carcinogenic properties [3,4]. Therefore, a lot of methods have been used to remove Cr(VI) from wastewater such as ion exchange [5,6], adsorption [7,8], photocatalyst [9,10], membrane separation [11,12], coagulation and precipitation [13,14], and solvent extraction [15]. Photocatalysts are commonly considered as the most promising and frequently used feasible strategy, owing to its easy operation, eco-friendly, low cost, regeneration, and high performance when compared to other approaches [16,17]. Various photocatalyst for the removal of Cr (VI) have been investigated, including active carbon [18], metal oxide nanoparticles [19,20], synthesized polymer beads [21] and agriculture waste [22]. Among these, iron oxide (Fe_3O_4) is one of the most widely studied due to its high efficiency, chemical stability, low cost, and availability [23,24]. However, after photodegradation, it is extremely difficult to separate the

catalyst from the solution, which would raise the operational costs [25,26]. In order to avoid this problem, some researchers used nanofibers to remove a variety of pollutants [27,28].

Electrospinning is a simple and efficient technique for fabricating polymer–inorganic nanocomposite fibers due to the higher mesoporosity and specific surface area [29,30]. Various nanomaterials can be introduced into the polymer matrix through the electrospinning process to improve the physical, chemical, and catalytic properties of the polymer fibers [31]. Due to its excellent characteristics, such as industrial availability, favorable chemical resistance, thermal resilience, strong mechanical properties, vast possibilities for surface functionalization, biocompatible and non-toxic composition, polyethersulfone (PES) has been used to manufacture nanofibers [32]. It has recently shown that incorporating two different types of nanomaterials into a polymer matrix has significant possible benefits in terms of improving property enhancement [33]. CNTs have excellent mechanical, thermal, electrical, and optical properties, as well as high aspect ratios [29,34]. Therefore, mixing iron oxide NPs with electrospun polymeric nanofibers can overcome the agglomeration and recycling problem of the nanoparticles. In addition, the mixture can be used as an efficient photocatalyst for the removal of heavy metal ions and development the magnetic nanofibers [35,36]. Recently, Hota et al. have reported the electrospinning fabrication of PAN/iron oxide for the removal performance of CR dye from aqueous solution [32]. In addition, Li et al. announced the electrospinning fabrication of a nylon 6/iron oxide composite nanofibers membrane for the removal of Cr(VI) ions from the aqueous solution [37]. Moreover, Mallon et al. fabricated the electrospun composite nanofibers containing carbon nanotubes and iron oxide (MWCNT-Fe_3O_4) [38].

In the present work, novel composite nanofibers were fabricated for the photodegradation of Cr(VI) from aqueous solutions, which can be easily separated from the aqueous solution. Photodegradation experiments were used to investigate the effects of pH, contact time, and initial concentration on Cr(VI). The electrospinning technique was also used to examine the incorporation of the respective MWCNT-Fe_3O_4 as filler nanomaterials into PES nanofibers. Furthermore, the preparation process and the photocatalytic mechanism of composite nanofibers for Cr(VI) were investigated. The morphology and structure of the composite nanofibers were characterized by scanning electronic microscope (SEM) and X-ray diffraction (XRD). The composite nanofiber showed promising potential for wastewater treatment.

2. Results and Discussion

Figure 1 shows the SEM images of PES, PES/MWCNTs-Fe_3O_4, MWCNTs-Fe_3O_4@PES composite nanofiber before and after photodegradation. The surface morphology of the PES nanofiber is uniform without beads with an average size of 105 $\pm$ 15 nm. The incorporation of MWCNTs and Fe_3O_4 NPs in the PES nanofiber can be seen in Figure 1b. The NPs can be seen inside the nanofiber with an average size of 95 $\pm$ 10 nm, due to the electrically conductive nature of MWCNT, which enhances solution conductivity, resulting in smaller nanofiber diameters. The successful fabrication of MWCNTs-Fe_3O_4@PES nanofibers before and after photodegradation is depicted in Figure 1c,d. It was observed that the NPs are agglomerated to each other and crosslinked well to the nanofiber even after photodegradation of Cr(VI).

In order to confirm the presence of NPs in the synthesized composite nanofiber, XRD analysis has been done as shown in Figure 2. The peaks at 30°, 35°, 44°, 57°, and 63° correspond to the presence of Fe_3O_4. The broad peaks of PES nanofiber at 2θ of 13.5°, 30° and 42.3°, indicating the amorphous nature of PES [39]. For the MWCNTs-Fe_3O_4@PES composite nanofiber, peaks at 2θ = 25.5° correlate to the presence of MWCNTs, whereas the peak at 13.5° related to the PES nanofiber and the peaks at 30°, 35°, 44°, 57°, and 63° associated to the Fe_3O_4 NPs. In addition, after photodegradation the same diffraction peaks are observed indicated the stability of the composite nanofiber.

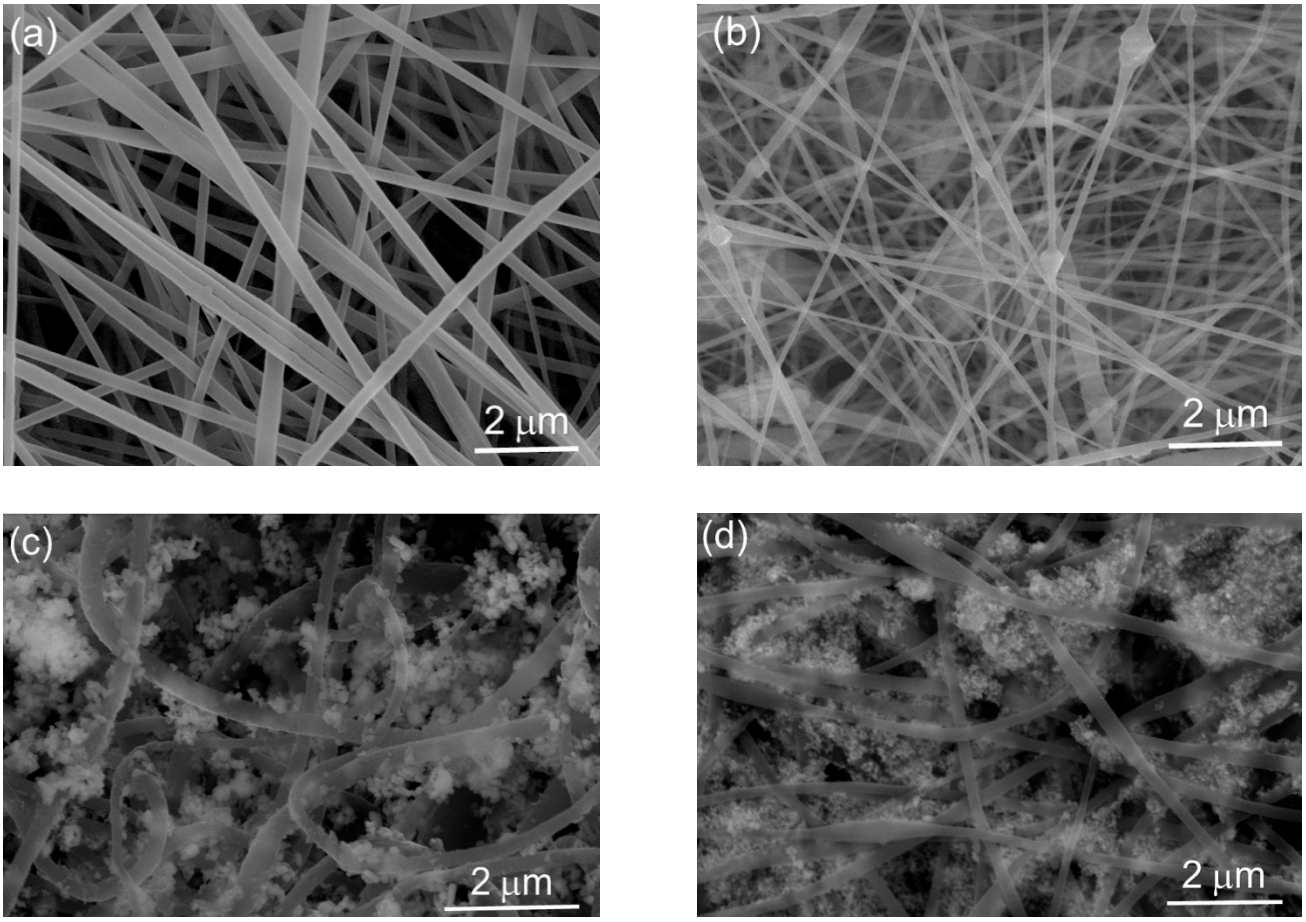

Figure 1. SEM images of (**a**) PES nanofiber, (**b**) PES/MWCNTs-Fe_3O_4, (**c**) MWCNTs-Fe_3O_4@PES and (**d**) MWCNTs-Fe_3O_4@PES composite nanofiber after photodegradation.

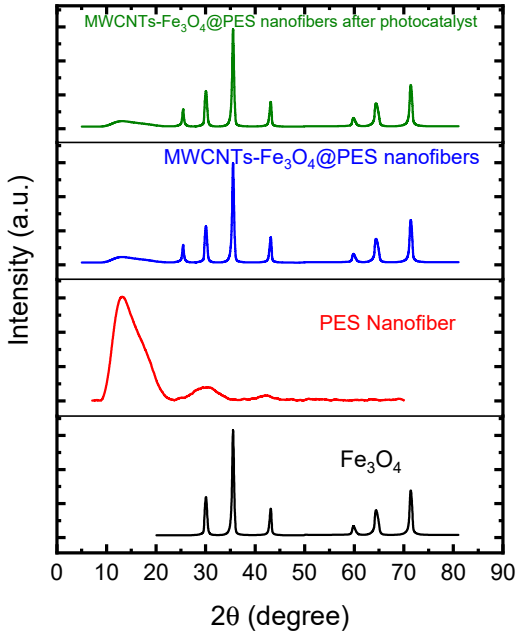

Figure 2. XRD patterns of Fe_3O_4, PES nanofiber, and MWCNTs-Fe_3O_4@PES composite nanofiber before and after photodegradation.

2.1. Photocatalytic Performance

Catalysts dose plays a crucial role in the photocatalysis process. The results depicted in Figure 3 exhibited that as the amount of MWCNTs increased, the photocatalytic efficiency of Cr(VI) increased with a fixed amount of Fe_3O_4 (1 wt.%) at pH 2, 80 min and 20 mgL^{-1} of Cr(VI). It is clear that the 3 and 5 wt.% of MWCNTs have the same photocatalytic efficiency, as the increase in the catalyst dose offers more binding sites, resulting in improving the photodegradation.

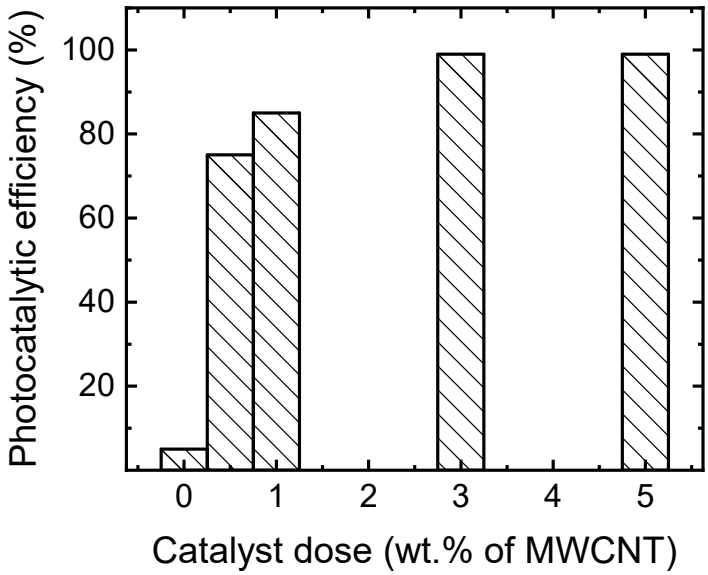

Figure 3. Effect of catalyst dose on the photocatalytic efficiency of Cr(VI) using the MWCNTs-Fe_3O_4@PES CNM.

During photocatalysis experiments, the contact time between photocatalysis and contaminants is critical for determining photocatalytic efficiency. The photocatalytic efficiency of Cr(VI) as a function of time using the PES nanofiber, PES/MWCNTs-Fe_3O_4 CNM, and MWCNTs-Fe_3O_4@PES CNM were determined as shown in Figure 4. All the experiments were conducted at 20 mgL^{-1} of Cr(VI) and pH 2. The results reveal that the maximum photocatalytic efficiency of Cr(VI) occurs at 80 min using the MWCNTs-Fe_3O_4@PES CNM under visible light, whereas for PES/MWCNTs-Fe_3O_4 CNM only 75% photocatalytic efficiency of Cr(VI) was achieved at the same condition. These results attributed to the large surface area and the large number of active sites in the case of MWCNTs-Fe_3O_4@PES CNM. In addition, both the composite nanofiber had higher photocatalytic efficiency than PES nanofiber.

The pH of a solution has a significant impact on the behaviour of photocatalyst against pollutants due to the surface charge of the photocatalyst, as well as the speciation of the metal ions in the solution [40]. The influence of pH on the photocatalytic efficiency of Cr(VI) using the MWCNTs-Fe_3O_4@PES CNM was established at various pH solutions in the range of 2–10 at 20 mgL^{-1} and 80 min as shown in Figure 5a. The results demonstrated that the highest photocatalytic efficiency of Cr(VI) occurs at a lower pH and decreased until 83% at pH 10. This result attributed to the electrostatic interactions between the positively charged iron oxide and the negatively charged of Cr(VI) that exists as an oxyanion (CrO_4^{-2}, $Cr_2O_7^{-2}$, or $HCrO_4^{-}$) in acidic media [40,41]. In addition, the electrostatic repulsions between the photocatalyst and the dichromate ions, resulting in a decline in photocatalytic efficiency of Cr(VI) in the basic medium. Furthermore, various concentrations (20, 40, 60, 80, and 100 mgL^{-1}) of Cr(VI) at pH 2 using the MWCNTs-Fe_3O_4@PES CNM were used at a contact time of 80 min, to determine the initial concentration effect, as shown in Figure 5b. The photocatalytic efficiency of Cr(VI) decreased from 99 to 66 % when the concentration increased from 20–100 mgL^{-1}, due to the binding sites being occupied by

Cr(VI), leaving little available binding sites for the photocatalyst process, resulting in a decrease in photocatalytic efficiency [42–44].

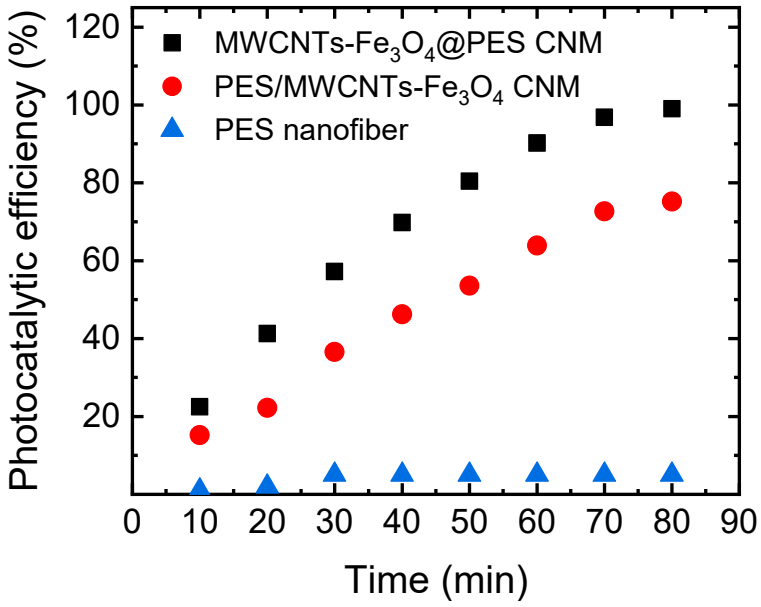

Figure 4. Photocatalytic efficiency of Cr(VI) using PES nanofiber, PES/MWCNTs-Fe_3O_4 CNM, and MWCNTs-Fe_3O_4@PES CNM.

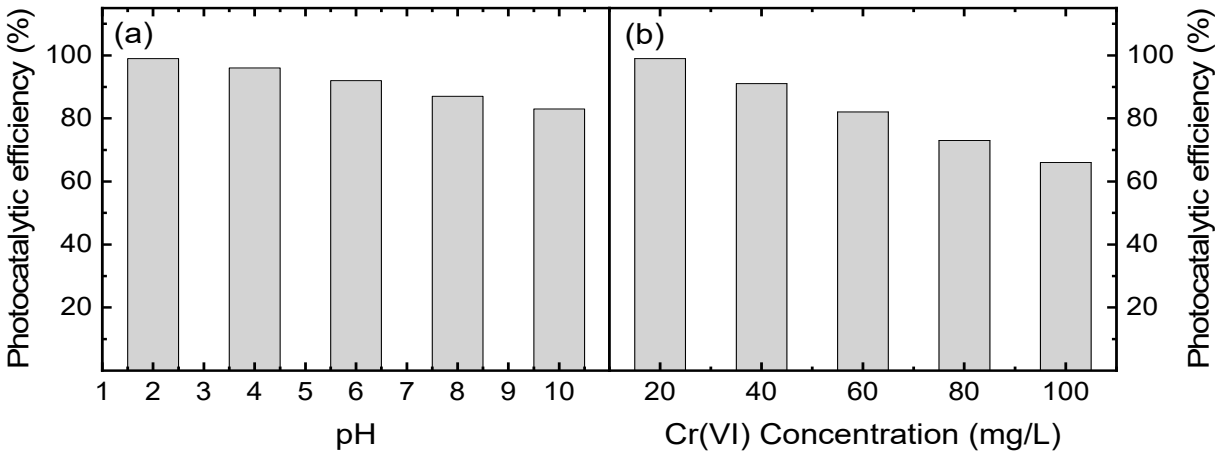

Figure 5. The effect of (**a**) pH and (**b**) concentration on the photocatalytic efficiency of Cr(VI) using the MWCNTs-Fe_3O_4@PES CNM.

2.2. Reusability of the Photocatalysis

For cost-effectiveness, the reusability and stability of catalyst materials is a critical factor. The regeneration of CNM was performed at pH 2, 20 mg L^{-1} and 80 min, as shown in Figure 6. After each cycle, the composite nanofiber treated with HCl solution and then washed with purified water. The results show that the composite nanofibers were effectively reused without significant reduction in the photocatalytic efficiency of Cr(VI) after 5 cycles, reaching 99%. In addition, Table 1 shows the photodegradation of Cr(VI) using different photocatalysis composite nanofiber, to compare the catalytic activity of different photocatalysis for Cr(VI) photodegradation under visible light irradiation.

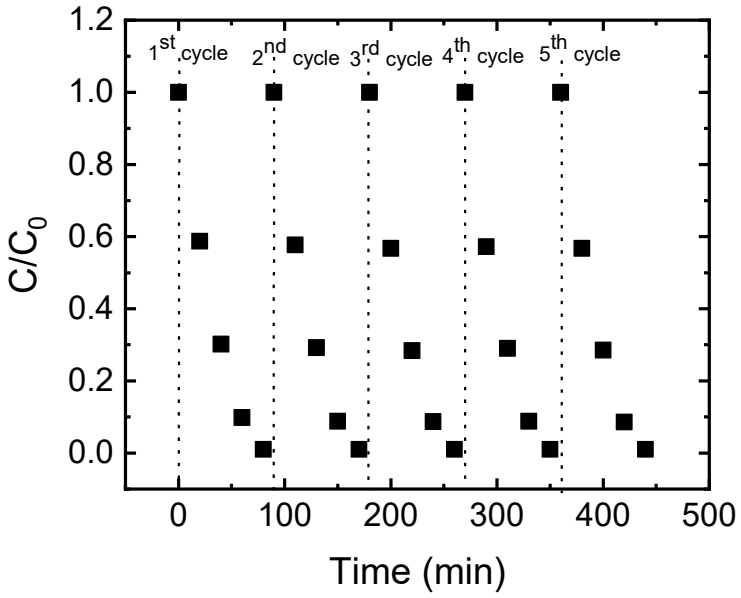

Figure 6. Reusability of the composite nanofibers for the photodegradation of Cr(VI) after 5 cycles.

Table 1. Comparison of visible light photodegradation of Cr(VI) using different composite nanofiber photocatalysis.

Catalyst	Concentration (mg L^{-1})	Photodegradation Efficiency (%)	Lamp Power (W)	Time (min)	Reference
CNF@SnS_2	50	100	300	90	[45]
PANI-CdS QDs	10	97	300	480	[46]
TiO_2/Ag	10	100	500	180	[47]
TiO_2@PAN	5	99	300	30	[48]
PDPB-ZnO	10	99	-	90	[49]
PES/MWCNTs-Fe_3O_4	20	75	125	80	This work
MWCNTs-Fe_3O_4@PES	20	100	125	80	This work

3. Experimental

3.1. Materials

Polyethersulfone (PES) was purchased from BASF, Germany. Glutaraldehyde (GA) 50%, potassium dichromate ($K_2Cr_2O_7$), iron(II) chloride, iron(III) acetylacetonate, ethylenediamine, dimethylformamide (DMF), acetylacetone, sodium acetate, ethanol, sodium hydroxide, hydrochloric acid, iron oxide magnetic, and ferric chloride was purchased from Sigma Aldrich. MWCNTs (average length of 0.5–2 µm, and diameter ranges from 30 to 50 nm), were synthesized and the procedure is described elsewhere [50,51]. All the chemicals were used without further purifications.

3.2. Preparation of Iron Oxide Nanoparticles by Hydrothermal Process

First, 1.7 g of iron chloride was dissolved in 10 mL distilled water, and then 1.9 mL of Acetylacetone was added to the solution after 15 min. After that, 6.25 g of sodium acetate was added to the solution with slow stirring. The solution was cooled to a temperature rang about 0–5 °C, which tends to result red crystalline. After that, iron (III) acetylacetonate was recrystallized from absolute ethanol. The prepared material was dissolved in 70 mL deionized water, and ethylene diamine was added into the solution under stirring condition to keep the pH between 10 and 11. After that, the resulting suspension transferred into a Teflon lined autoclave, where the hydrothermal reaction was carried out for 12 h at 150 °C. After the completion of the reaction, the mixture was washed several times with distilled

water and finally with alcohol and then isolated by centrifugation. The precipitate was then dried in an electric oven at 60 °C for further use.

3.3. Synthesis of Electrospun Composite Nanofiber

The PES nanofibers were fabricated via the electrospinning technique. Briefly, 1 g of PES was added into 4 mL of DMF and mixed by magnetic stirrer until the solution was homogeneous. The prepared PES solution was poured into a 6 mL plastic syringe. The electrospinning was performed at 15 kV, 1 mL·h^{-1} of solution flow rate and 20 cm distance from needle to the collector. The obtained nanofibers were taken off from the aluminium foil for further use. For the composite nanofiber (PES/MWCNTs-Fe_3O_4), 1 wt.% of MWCNTs and Fe_3O_4 w.r.t. the polymer weight were prepared by blending with PES and electrospun as the PES nanofibers. For the preparation of the MWCNTs-Fe_3O_4 on the surface of PES nanofibers, different amounts of MWCNTs (0.5, 1, 3 and 5 wt.%) and 1 wt.% of Fe_3O_4 have been prepared as follow. The PES nanofibers were immersed in a crosslinking medium containing 100 mL purified water with 2.5 wt% GA for 24 h [52]. Then, the GA was separated, and the composite nanofiber washed and dried. After that, 2 mL of the prepared suspension mixture of MWCNTs and Fe_3O_4 was applied to the nanofibers for 24 h. Finally, the CNM was washed out with deionized water and ethanol, and then dried for further use.

3.4. Characterization

The morphology of the synthesized composite nanofibers membrane (CNM) was examined using a scanning electron microscope (SEM, Gemini Zeiss-Ultra 55, ZEISS, Jena, Germany). The average diameter of the CNMs were calculated using Image J software and calculated by selecting the fiber diameter observed on the SEM image. The X-ray diffraction (XRD) patterns were conducted using (D8-Advance, Bruker, Billerica, MA, USA) varying from 3° to 30° with Cu-Kα radiation to establish the composition and crystallinity of Fe_3O_4 and the composite nanofiber membrane. UV–Vis Absorbance (LAMBDA 750, Perkin Elmer, Solingen, Germany) was used to determine the concentration of Cr(VI) in aqueous solutions.

3.5. Photocatalysis Experiments

The photocatalysis experiments were carried out to investigate the effect of contact time, initial Cr(VI) concentrations and pH values (2–10) under visible light (125 W xenon lamp) using the composite nanofiber membrane for the photodegradation of Cr(VI). Photocatalysis experiments were conducted in petri dish, with50 mL of Cr(VI) concentration (20–100 mgL^{-1}) and 20 mg of composite nanofiber. The fabricated nanofibers was placed into the petri dish and mixed with Cr(VI) solution at room temperature in the dark for 30 min to assure that the adsorption equilibrium of Cr(VI) was reached. After equilibration, the solution was irradiated with visible light, where the distance between the light source and the CNM is 20 cm. After that, 3 mL of the suspension was taken at scheduled intervals for the analysis. Potassium dichromate (K_2Cr_2O7) was used to prepare different concentration of Cr (VI). The Cr(VI) concentration in the solution was determined by recording the absorbance at 350 nm on a UV–Vis Absorbance (LAMBDA 750, Perkin Elmer).The photocatalytic performance of Cr(VI) is given as follows:

$$\text{Photocatalytic efficiency } (\%) = \left(\frac{C_0 - C_t}{C_0}\right) \times 100 \quad (1)$$

where C_0 and C_t is the initial and final Cr(VI) concentration (mg/L).

4. Conclusions

The PES/MWCNTs-Fe_3O_4 and MWCNTs-Fe_3O_4@PES composite nanofibers were successfully prepared by the electrospinning technique. The NPs were blending to the PES solution and/or loaded to the surface of the nanofiber to prepare the composite

nanofibers. The prepared MWCNTs-Fe_3O_4@PES composite nanofibers have a higher photodegradation efficiency of Cr(VI) than the PES/MWCNTs-Fe_3O_4 and PES alone. The maximum photodegradation of Cr(VI) was 99% after 80 min. The photodegradation efficiency was highest at acidic pH 2 (99%) whereas 83% was achieved at pH 10 due to the electrostatic interactions between active sites on the surface of the catalyst with positive charges of $HCrO_4^-$. In addition, the photocatalytic efficiency of Cr(VI) decreased from 99 to 66% when the concentration increased from 20–100 mgL^{-1}. Moreover, after 5 cycles of photodegradation of Cr(VI), the composite nanofibers demonstrated high performance, stability, and reusability. The results demonstrated that the catalysts materials have a potential photodegradation of Cr(VI) from industrial wastewater.

Author Contributions: A.M. and S.Y.: conceptualization, methodology, investigation, writing—original draft, writing—review and editing; S.A., B.M.K., and M.A.A.: Formal Analysis; writing—review and editing; M.S., S.V., S.T.; review and editing. All authors have read and agreed to the published version of the manuscript.

Funding: Not applicable.

Data Availability Statement: Not applicable.

Acknowledgments: Not applicable.

Conflicts of Interest: The authors declare no conflict of interest.

References

1. Joshi, K.M.; Shrivastava, V.S. Photocatalytic degradation of Chromium (VI) from wastewater using nanomaterials like TiO_2, ZnO, and CdS. *Appl. Nanosci.* **2011**, *1*, 147–155. [CrossRef]
2. Bhati, A.; Anand, S.R.; Saini, D.; Sonkar, S.K. Sunlight-induced photoreduction of Cr(VI) to Cr(III) in wastewater by nitrogen-phosphorus-doped carbon dots. *NPJ Clean Water* **2019**, *2*, 12. [CrossRef]
3. Wang, K.; Qiu, G.; Cao, H.; Jin, R. Removal of Chromium(VI) from Aqueous Solutions Using Fe_3O_4 Magnetic Polymer Microspheres Functionalized with Amino Groups. *Materials* **2015**, *8*, 8378–8391. [CrossRef] [PubMed]
4. Bai, X.; Du, Y.; Xue, W.; Hu, X.; Fan, J.; Li, J.; Liu, E. Enhancement of the photocatalytic synchronous removal of Cr(vi) and RhB over RP-modified flower-like SnS2. *Nanoscale Adv.* **2020**, *2*, 4220–4228. [CrossRef]
5. Kononova, O.; Bryuzgina, G.; Apchitaeva, O.; Kononov, Y. Ion exchange recovery of chromium (VI) and manganese (II) from aqueous solutions. *Arab. J. Chem.* **2019**, *12*, 2713–2720. [CrossRef]
6. Liu, S.; Cao, L.; Tian, X.; Li, X.; Liao, L.; Zhao, C. Enhanced removal of Cr(VI) using a modified environment-friendly adsorbent. *Water Sci. Technol.* **2021**, *83*, 678–688. [CrossRef] [PubMed]
7. Egbosiuba, T.C.; Abdulkareem, A.S.; Kovo, A.S.; Afolabi, E.A.; Tijani, J.O.; Bankole, M.T.; Bo, S.; Roos, W.D. Adsorption of Cr(VI), Ni(II), Fe(II) and Cd(II) ions by KIAgNPs decorated MWCNTs in a batch and fixed bed process. *Sci. Rep.* **2021**, *11*, 1–20. [CrossRef]
8. Wei, Y.; Chen, W.; Liu, C.; Wang, H. Facial Synthesis of Adsorbent from Hemicelluloses for Cr(VI) Adsorption. *Molecules* **2021**, *26*, 1443. [CrossRef]
9. Abdel-Mottaleb, M.; Khalil, A.; Osman, T.; Khattab, A. Removal of hexavalent chromium by electrospun PAN/GO decorated ZnO. *J. Mech. Behav. Biomed. Mater.* **2019**, *98*, 205–212. [CrossRef]
10. Mohamed, A.; Nasser, W.; Osman, T.; Toprak, M.; Muhammed, M.; Uheida, A. Removal of chromium (VI) from aqueous solutions using surface modified composite nanofibers. *J. Colloid Interface Sci.* **2017**, *505*, 682–691. [CrossRef]
11. Astolfi, M.L.; Ginese, D.; Ferrante, R.; Marconi, E.; Girelli, A.M.; Canepari, S. On-Line Separation and Determination of Trivalent and Hexavalent Chromium with a New Liquid Membrane Annular Contactor Coupled to Inductively Coupled Plasma Optical Emission Spectrometry. *Processes* **2021**, *9*, 536. [CrossRef]
12. Khalil, A.M.; Schäfer, A.I. Cross-linked β-cyclodextrin nanofiber composite membrane for steroid hormone micropollutant removal from water. *J. Membr. Sci.* **2021**, *618*, 118228. [CrossRef]
13. Mahringer, D.; Zerelli, S.S.; Dippon, U.; Ruhl, A.S. Pilot scale hexavalent chromium removal with reduction, coagulation, filtration and biological iron oxidation. *Sep. Purif. Technol.* **2020**, *253*, 117478. [CrossRef]
14. Golbaz, S.; Jafari, A.J.; Rafiee, M.; Kalantary, R.R. Separate and simultaneous removal of phenol, chromium, and cyanide from aqueous solution by coagulation/precipitation: Mechanisms and theory. *Chem. Eng. J.* **2014**, *253*, 251–257. [CrossRef]
15. Ying, Z.; Ren, X.; Li, J.; Wu, G.; Wei, Q. Recovery of chromium(VI) in wastewater using solvent extraction with amide. *Hydrometallurgy* **2020**, *196*, 105440. [CrossRef]
16. Mohamed, A.; Ghobara, M.M.E.; Abdelmaksoud, M.; Mohamed, G.G. A novel and highly efficient photocatalytic degradation of malachite green dye via surface modified polyacrylonitrile nanofibers/biogenic silica composite nanofibers. *Sep. Purif. Technol.* **2019**, *210*, 935–942. [CrossRef]

17. Khalil, A.; Nasser, W.S.; Osman, T.; Toprak, M.S.; Muhammed, M.; Uheida, A. Surface modified of polyacrylonitrile nanofibers by TiO_2/MWCNT for photodegradation of organic dyes and pharmaceutical drugs under visible light irradiation. *Environ. Res.* **2019**, *179*, 108788. [CrossRef]
18. Sabri, M.; Sara, Z.; Al-Sayah, M.; Ibrahim, T.; Khamis, M.; El-Kadri, O. Simultaneous Adsorption and Reduction of Cr(VI) to Cr(III) in Aqueous Solution Using Nitrogen-Rich Aminal Linked Porous Organic Polymers. *Sustainability* **2021**, *13*, 923. [CrossRef]
19. Kumar, H.; Sinha, S.K.; Goud, V.V.; Das, S. Removal of Cr(VI) by magnetic iron oxide nanoparticles synthesized from extracellular polymeric substances of chromium resistant acid-tolerant bacterium Lysinibacillus sphaericus RTA-01. *J. Environ. Health Sci. Eng.* **2019**, *17*, 1001–1016. [CrossRef]
20. Mohamed, A.; Osman, T.; Toprak, M.; Muhammed, M.; Yilmaz, E.; Uheida, A. Visible light photocatalytic reduction of Cr(VI) by surface modified CNT/titanium dioxide composites nanofibers. *J. Mol. Catal. A Chem.* **2016**, *424*, 45–53. [CrossRef]
21. Mulani, K.; Patil, V.; Chavan, N.; Donde, K. Adsorptive removal of chromium(VI) using spherical resorcinol-formaldehyde beads prepared by inverse suspension polymerization. *J. Polym. Res.* **2019**, *26*, 41. [CrossRef]
22. Shen, X.; Yang, Y.; Song, B.; Chen, F.; Xue, Q.; Shan, S.; Li, S. Magnetically recyclable and remarkably efficient visible-light-driven photocatalytic hexavalent chromium removal based on plasmonic biochar/bismuth/ferroferric oxide heterojunction. *J. Colloid Interface Sci.* **2021**, *590*, 424–435. [CrossRef]
23. Ge, T.; Jiang, Z.; Shen, L.; Li, J.; Lu, Z.; Zhang, Y.; Wang, F. Synthesis and application of Fe_3O_4/$FeWO_4$ composite as an efficient and magnetically recoverable visible light-driven photocatalyst for the reduction of Cr(VI). *Sep. Purif. Technol.* **2021**, *263*, 118401. [CrossRef]
24. Liu, F.; Zhang, W.; Tao, L.; Hao, B.; Zhang, J. Simultaneous photocatalytic redox removal of chromium(vi) and arsenic(iii) by hydrothermal carbon-sphere@nano-Fe_3O_4. *Environ. Sci. Nano* **2019**, *6*, 937–947. [CrossRef]
25. Khalil, A.; Aboamera, N.M.; Nasser, W.S.; Mahmoud, W.H.; Mohamed, G.G. Photodegradation of organic dyes by PAN/SiO_2-TiO_2-NH_2 nanofiber membrane under visible light. *Sep. Purif. Technol.* **2019**, *224*, 509–514. [CrossRef]
26. Mohamed, A.; Salama, A.; Nasser, W.S.; Uheida, A. Photodegradation of Ibuprofen, Cetirizine, and Naproxen by PAN-MWCNT/TiO_2–NH_2 nanofiber membrane under UV light irradiation. *Environ. Sci. Eur.* **2018**, *30*, 47. [CrossRef] [PubMed]
27. Uheida, A.; Mohamed, A.; Belaqziz, M.; Nasser, W.S. Photocatalytic degradation of Ibuprofen, Naproxen, and Cetirizine using PAN-MWCNT nanofibers crosslinked TiO_2-NH_2 nanoparticles under visible light irradiation. *Sep. Purif. Technol.* **2019**, *212*, 110–118. [CrossRef]
28. Mohamed, A.; Yousef, S.; Nasser, W.S.; Osman, T.A.; Knebel, A.; Sánchez, E.P.V.; Hashem, T. Rapid photocatalytic degradation of phenol from water using composite nanofibers under UV. *Environ. Sci. Eur.* **2020**, *32*, 1–8. [CrossRef]
29. Mohamed, A.; Yousef, S.; Abdelnaby, M.A.; Osman, T.; Hamawandi, B.; Toprak, M.; Muhammed, M.; Uheida, A. Photocatalytic degradation of organic dyes and enhanced mechanical properties of PAN/CNTs composite nanofibers. *Sep. Purif. Technol.* **2017**, *182*, 219–223. [CrossRef]
30. Karim, S.A.; Mohamed, A.; Abdel-Mottaleb, M.M.; Osman, T.A.; Khattab, A. Mechanical Properties and the Characterization of Polyacrylonitrile/Carbon Nanotube Composite Nanofiber. *Arab. J. Sci. Eng.* **2018**, *43*, 4697–4702. [CrossRef]
31. Mohamed, A.; Nasser, W.S.; Kamel, B.M.; Hashem, T. Photodegradation of phenol using composite nanofibers under visible light irradiation. *Eur. Polym. J.* **2019**, *113*, 192–196. [CrossRef]
32. Patel, S.; Hota, G. Iron oxide nanoparticle-immobilized PAN nanofibers: Synthesis and adsorption studies. *RSC Adv.* **2016**, *6*, 15402–15414. [CrossRef]
33. Yazdi, M.G.; Ivanic, M.; Mohamed, A.; Uheida, A. Surface modified composite nanofibers for the removal of indigo carmine dye from polluted water. *RSC Adv.* **2018**, *8*, 24588–24598. [CrossRef]
34. Abdel-Mottaleb, M.; Khalil, A.; Karim, S.; Osman, T.; Khattab, A. High performance of PAN/GO-ZnO composite nanofibers for photocatalytic degradation under visible irradiation. *J. Mech. Behav. Biomed. Mater.* **2019**, *96*, 118–124. [CrossRef] [PubMed]
35. Salama, A.; Mohamed, A.; Aboamera, N.M.; Osman, T.; Khattab, A. Characterization and mechanical properties of cellulose acetate/carbon nanotube composite nanofibers. *Adv. Polym. Technol.* **2017**, *37*, 2446–2451. [CrossRef]
36. Mohamed, A.; Khalil, A.M.; Osman, T.; Kamel, B.M. Development and manufacturing an automated lubrication machine test for nano grease. *J. Mater. Res. Technol.* **2020**, *9*, 2054–2062. [CrossRef]
37. Kim, H.J.; Pant, H.R.; Park, C.H.; Tijing, L.; Choi, N.J.; Kim, C.S. Hydrothermal growth of mop-brush-shaped ZnO rods on the surface of electrospun nylon-6 nanofibers. *Ceram. Int.* **2013**, *39*, 3095–3102. [CrossRef]
38. van Deventer, N.; Mallon, P.E. Electrospun Nanocomposite Nanofibres with Magnetic Nanoparticle Decorated Carbon Nanotubes. *Macromol. Symp.* **2018**, *378*. [CrossRef]
39. Laghaei, M.; Sadeghi, M.; Ghalei, B.; Shahrooz, M. The role of compatibility between polymeric matrix and silane coupling agents on the performance of mixed matrix membranes: Polyethersulfone/MCM-41. *J. Membr. Sci.* **2016**, *513*, 20–32. [CrossRef]
40. Maponya, T.; Ramohlola, K.; Kera, N.; Modibane, K.; Maity, A.; Katata-Seru, L.; Hato, M. Influence of Magnetic Nanoparticles on Modified Polypyrrole/*m*-Phenylediamine for Adsorption of Cr(VI) from Aqueous Solution. *Polymers* **2020**, *12*, 679. [CrossRef]
41. Muhammad, A.; Shah, A.U.H.A.; Bilal, S. Effective Adsorption of Hexavalent Chromium and Divalent Nickel Ions from Water through Polyaniline, Iron Oxide, and Their Composites. *Appl. Sci.* **2020**, *10*, 2882. [CrossRef]
42. Zhang, Q.; Jiang, X.; Kirillov, A.; Zhang, Y.; Hu, M.; Liu, W.; Yang, L.; Fang, R.; Liu, W. Covalent Construction of Sustainable Hybrid UiO-66-NH2@Tb-CP Material for Selective Removal of Dyes and Detection of Metal Ions. *ACS Sustain. Chem. Eng.* **2019**, *7*, 3203–3212. [CrossRef]

43. Yang, Z.; Zhu, L.; Chen, L. Selective adsorption and separation of dyes from aqueous solution by core-shell structured NH2-functionalized UiO-66 magnetic composites. *J. Colloid Interface Sci.* **2019**, *539*, 76–86. [CrossRef] [PubMed]
44. Ahmadijokani, F.; Mohammadkhani, R.; Ahmadipouya, S.; Shokrgozar, A.; Rezakazemi, M.; Molavi, H.; Aminabhavi, T.M.; Arjmand, M. Superior chemical stability of UiO-66 metal-organic frameworks (MOFs) for selective dye adsorption. *Chem. Eng. J.* **2020**, *399*, 125346. [CrossRef]
45. Zhong, Y.; Qiu, X.; Chen, D.; Li, N.; Xu, Q.; Li, H.; He, J.; Lu, J. Flexible Electrospun Carbon Nanofiber/Tin(IV) Sulfide Core/Sheath Membranes for Photocatalytically Treating Chromium(VI)-Containing Wastewater. *ACS Appl. Mater. Interfaces* **2016**, *8*, 28671–28677. [CrossRef]
46. Talooki, E.F.; Ghorbani, M.; Rahimnejad, M.; Lashkenari, M.S. Evaluation of a visible light-responsive polyaniline nanofiber-cadmium sulfide quantum dots photocathode for simultaneous hexavalent chromium reduction and electricity generation in photo-microbial fuel cell. *J. Electroanal. Chem.* **2020**, *873*, 114469. [CrossRef]
47. Wang, L.; Zhang, C.; Gao, F.; Mailhot, G.; Pan, G. Algae decorated TiO_2/Ag hybrid nanofiber membrane with enhanced photocatalytic activity for Cr(VI) removal under visible light. *Chem. Eng. J.* **2017**, *314*, 622–630. [CrossRef]
48. Cai, J.; Li, H. Electrospun polymer nanofibers coated with TiO_2 hollow spheres catalyze for high synergistic photo-conversion of Cr(VI) and As(III) using visible light. *Chem. Eng. J.* **2020**, *398*, 125644. [CrossRef]
49. Ghosh, S.; Remita, H.; Basu, R.N. Visible-light-induced reduction of Cr(VI) by PDPB-ZnO nanohybrids and its photoelectrochemical response. *Appl. Catal. B Environ.* **2018**, *239*, 362–372. [CrossRef]
50. Mohamed, A.; Osman, T.A.; Khattab, A.; Zaki, M. Tribological Behavior of Carbon Nanotubes as an Additive on Lithium Grease. *J. Tribol.* **2014**, *137*, 011801. [CrossRef]
51. Yousef, S.; Mohamed, A. Mass production of CNTs using CVD multi-quartz tubes. *J. Mech. Sci. Technol.* **2016**, *30*, 5135–5141. [CrossRef]
52. Abdel-Mottaleb, M.M.; Mohamed, A.; Karim, S.A.; Osman, T.A.; Khattab, A. Preparation, characterization, and mechanical properties of polyacrylonitrile (PAN)/graphene oxide (GO) nanofibers. *Mech. Adv. Mater. Struct.* **2018**, *27*, 346–351. [CrossRef]